47th AIAA Aerospace Sciences Meeting Including The New Horizons Forum and Aerospace Exposition
5 - 8 January 2009, Orlando, Florida

AIAA 2009-541

Flow over Delta Wing with Low Dorsal Fin–PIV Study

Xuanshi Meng*, Zhide Qiao†, Chao Gao‡
Northwestern Polytechnical University, Xi'an 710072, China
Shijun Luo§, and Feng Liu¶
University of California, Irvine, CA 92697-3975

A recent theoretical and experimental work done on the vortex flow over slender flat-plate delta wing with low dorsal fin is reviewed, and a particle image velocimetry (PIV) study is conducted to further the investigation. The distributions of the vorticity component normal to the cross-flow planes show significant flow asymmetry and non-conicity over the wing-fin combination at a high angle of attack and enhance the validation of the theoretical prediction that adding a low dorsal fin to the wing may destabilize the symmetric and conical vortex pair. Ideals for further work are suggested.

Nomenclature

b	=	wing span
c_0	=	wing root chord
C_n	=	yawing-moment coefficient, yawing moment about Z-axis/$q_\infty Sb$
h_L	=	local height of dorsal fin
K	=	Sychev similarity parameter, $\tan\alpha/\tan\epsilon$
q_∞	=	free-stream dynamic pressure
S	=	wing area
s	=	local semi-span of wing
U_∞	=	free-stream velocity
v, w	=	cross-flow velocity components
X, Y, Z	=	balance body axes, Fig. 4
x, y, z	=	body axes of the wing
α	=	angle of attack
ϵ	=	semi-apex angle of wing
β	=	sideslip angle
ω_x	=	axial vorticity, $\partial w/\partial y - \partial v/\partial z$

I. Introduction

Symmetric separation vortices over slender bodies may become asymmetric as the angle of attack is increased beyond a certain value, causing asymmetric forces even at symmetric flight conditions. The transition of the vortex pattern from being symmetric to asymmetric over symmetric bodies under symmetric flow conditions is a fascinating fluid dynamics problem and of major importance for the performance and

*Graduate Student, Department of Fluid Mechanics.
†Professor, Department of Fluid Mechanics.
‡Professor and Associate Director, Aerodynamic Design and Research National Laboratory.
§Researcher, Department of Mechanical and Aerospace Engineering.
¶Professor, Department of Mechanical and Aerospace Engineering. Associate Fellow AIAA.

Copyright © 2009 by the American Institute of Aeronautics and Astronautics, Inc. All rights reserved.

control of high-maneuverability flight vehicles that favor the use of slender bodies. Excellent reviews on this subject can be found in the paper by Ericsson.[1]

Shanks[2] performed tests of highly swept delta wings with semi-apex angles of 6 to 20 degrees at high angles of attack up to 40 degrees over a range of Reynolds numbers from 0.9×10^6 to 2.4×10^6 based on wing root chord. His measurements showed the appearance of significant rolling moments at angles of attack above 24 degrees and zero sideslip for models whose semi-apex angles are less than 12 degrees. Shanks' experiment led to the belief that the vortex flow over a low aspect-ratio delta wing with sharp leading-edges, like the flow over slender pointed bodies of revolution, would become asymmetric at high angles of attack and zero sideslip before vortex breakdown occurs over the wing.[3,4] Later, Stahl, Mahmood, and Asghar[5] performed water tunnel and wind tunnel experiments and concluded based on their force measurements and flow visualization that the vortex flow over slender delta wings with sharp leading edges remained symmetric at all angles of attack until vortex breakdown occurred on the wing. That conclusion seemingly contradicted the observations by Shanks. Ericsson,[1] however, noticed that Shanks' wing model differed from that by Stahl et al.[5] in that Shanks' model contained a low center spline or 'fuselage bump' on the leeside of the wing. Ericsson claimed that the vortex asymmetry observed in Shanks' experiment was not due to hydrodynamic instability but rather likely due to asymmetric reattachment in the presence of the centerline spline.

Cai, Liu, and Luo[6] developed a vortex stability theory for slender conical bodies and showed by their analytical methods that vortices over a flat-plate delta wing at zero sideslip are conical, symmetric, and stable for all angles of attack but adding a low dorsal fin to the wing would destabilize the vortices and therefore render the originally symmetric vortices asymmetric and/or non-conical. The flow would recover symmetry only when the fin height is increased to a critical level. The forward half of the Shanks' models approximated conical bodies. By examining the data in Shanks' test and comparing with their predicted range of fin heights needed to destabilize the vortex flow, Cai et al.[6] suggested that the vortex asymmetries observed in Shanks' experiments were caused by the destabilizing effect of the center spline, which functions as a low height dorsal fin on Shanks' flat-plate delta wings.

It may be argued that the 'bump' on Shanks' test model is not exactly a flat-plate fin as assumed in the theory by Cai et al.[6] Models of strictly slender and conical flat-plate fins added to a sharp-edged flat-plate delta wing were made. Investigations by the smoke-laser-sheet visualizations[7] and the six-component internal strain-gage-balance measurements[8] yielded results agreeable to the theory.[6] However, the information is limited by the inherent nature of the instruments. A particle image velocimetry (PIV) study is perfomed in this paper to promote the validation.

The following sections briefly review the theoretical results,[6] the smoke-laser-sheet results[7] and the force-measurement results.[8] The PIV experimental setup is described. The PIV experimental results are then presented and discussed. Conclusions are lastly drawn.

II. Review of Theoretical Results and Choice of Experimental Parameters

The theoretical model for the conical wing and dorsal fin combination is shown in Fig. 1. The flow is assumed steady, incompressible, inviscid, conical, and slender. The vortex sheet connecting the concentrated vortex line and the wing leading-edge is neglected. The vortex shedded from the fin leading edge, if any, is also neglected. The perturbations are small. No vortex breakdown occurs over the wing surfaces.

Cai et al.[6] showed that adding a vertical flat-plate dorsal fin of small to moderate height to the flat-plate delta wing has an effect of decreasing the stability of the leading-edge vortex pair. Figure 1 reproduces results from Ref. 6 in the form of the maximum real part of the eigenvalues for the vortex-flow stability under small symmetric and anti-symmetric perturbations versus the non-dimensional fin local height based on the wing local semi-span, i.e., h_L/s, for the Sychev similarity parameters[9] $K = 4.0$. A positive real part of the eigenvalue means instability of the vortex system. Figure 1 shows that the dorsal fin has a destabilizing effect on the symmetric vortex pair over the delta wing when $h_L/s < 1.306$ for $K = 4.0$. The initially stable symmetric vortices become unstable under anti-symmetric perturbations when the dorsal fin height is in the range $0.222 < h_L/s < 1.247$.

We design experiments to verify the theoretical predictions. A sharp-edged flat-plate delta wing of semi-apex angle $\epsilon = 7.5^\circ$ and four different flat-plate fin heights $h_L/s = 0.3, 0.6, 0.75$ and 1.5 are chosen in the experiments. Angle of attack of 30° yields the Sychev similarity parameters $K \approx 4.0$. According to Figure 1, the three wing-fin models of $h_L/s = 0.3, 0.6$ and 0.75 have positive maximum real part of the eigenvalues,

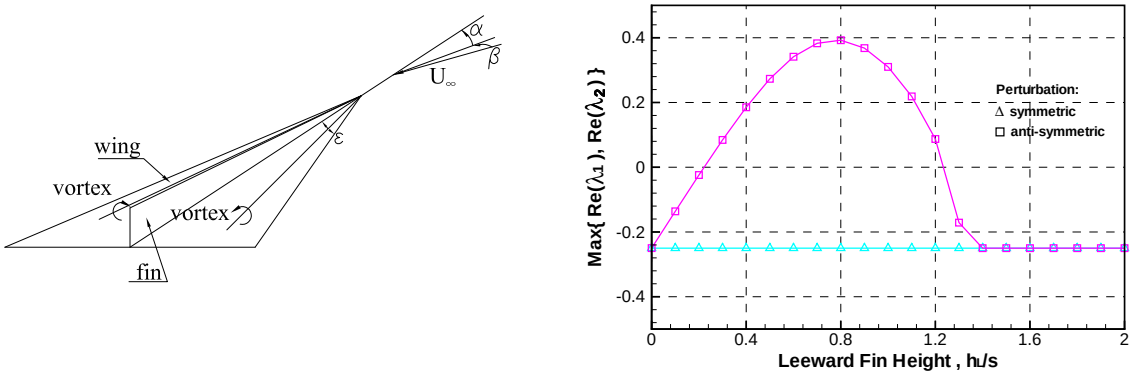

(a) theoretical model

(b) maximum real part of eigenvalues

Figure 1. Theoretical model and maximum real part of eigenvalues of stationary symmetric conical vortex pair over wing-fin combination, $K = 4.0$, $\beta = 0$.

indicating that the symmetric vortex pair over the wing with the three fins is unstable; while the model of $h_L/s = 1.5$ gives a negative maximum real part of the eigenvalues, indicating that the symmetric vortex pair over the wing with the high fin is stable.

III. Review of Smoke-Laser-Sheet Results

The smoke-laser-sheet visualizations[7] were conducted in a low-speed $3.5 \times 2.5 \times 12\ m$ wind tunnel at the Aerodynamic Design and Research National Laboratory, Northwestern Polytechnical University. The sweep angle of the wing is 82.5°. The wing root chord $c_0 = 990.6\ mm$. Two fin heights are chosen, $h_L/s = 0.75$ and 1.50. Three tested models are the wing alone, the wing+$0.75s$-fin and the wing+$1.5s$-fin combinations. $\alpha = 29.02°$. $K \approx 4.0$. $\beta = 0$. The wind speed $U_\infty = 4.5\ m/s$. The Reynolds number $Re = 2.99 \times 10^5$ based on the root chord of the wing.

The wing is made of a red pine plate of thickness 19.1 mm. The leading and trailing edges are beveled with a 20° angle from the windward side so that the leeward side of the wing is perfectly flat. For visualization purpose, the two fins are made of clear float glass. The fins have a thickness of 2 mm. The leading edges of the fins are blunt and have the shape of an isosceles trapezoid. Figure 2 shows a photograph of the test section layout. The smoke rake is located at a distance of 2080 mm upstream to the wing apex. The lens of the laser-sheet source is movable along a rail parallel to the wing root chord on the right side of the model. A 25-frames-per-second digital vidicom is mounted downstream in the test section to record the vortical flowfield.

The tip portion of all models up to $x/c_0 = 15.0\%$ is separately made for construction reasons. The tip is made of metal to maintain a sharp tip and high precision for a conical shape. The rest portion of the wing is common to all the three models. The dorsal fin is glued vertically to the upper surface of the wing in the wing symmetry plane. The models are made to very close tolerances and have a high surface finish. The model is rigidly held by a model support on the windward side.

Quantitative measurements of the vortex locations at each streamwise location are made by digitally overlapping the laser sheet vortex patterns to a grid that is separately photographed by placing a thin board with the grid on the wing in the same streamwise cross-section and with all other settings unchanged. The grid has a minimum measuring scale of 2 mm. Photographs of the vortices overlapped with the measuring grid are shown in Figure 3 for the three models at the cross-flow plane $x/c_0 = 0.54$. The vorex pair over the wing+$0.75s$-fin model is relatively asymmetric in comparison with that over the other two models.

Let $(y/s)_i$ and $(z/s)_i$ be the time-averaged local dimensionless coordinates of the vortex centers for the i-th cross-section of the wing. $i = 1 - 10$. The cross-sections are distributed uniformly between $x/c_0 = 0.3$

Figure 2. Photograph of the test section layout for smoke-laser-sheet experiments.

and 0.8. The coordinates are obtained by an average of the readings from twenty laser-sheet photographs that are equally-spaced in time out of a first ten-second video recording of the flow. Then their arithmetic mean values,$\bar{y}$ and $\bar{z}$, are calculated as follows.

$$\bar{y} = \sum_{i=1}^{I} (y/s)_i \, / I, \qquad \bar{z} = \sum_{i=1}^{I} (z/s)_i \, / I \tag{1}$$

where I is the total number of the measurement cross-sections along the wing axis. The arithmetic mean values of the vortex center coordinates $(\bar{y}, \bar{z})$ for the wing-alone, the wing+$0.75s$-fin, and the wing+$1.50s$-fin models are compared in Table 1.

Table 1. Comparison of the vortex-center mean coordinates $(\bar{y}, \bar{z})$ for the three models at $\alpha = 29.02^\circ$, $\beta = 0$.

Model	Port side		Starboard side	
	$\bar{y}$	$\bar{z}$	$\bar{y}$	$\bar{z}$
Wing	-0.61	0.576	0.659	0.564
Wing+$0.75s$-fin	-0.675	0.556	0.724	0.610
Wing+$1,50s$-fin	-0.695	0.562	0.705	0.549

The mean coordinates of the left and right vortices over the wing+$0.75s$-fin model exhibit asymmetry in comparison with those of the wing-alone and the wing+$1.50s$-fin models, which agrees with the analytical predictions.[6]

IV. Review of Force-Measurement Results

The force measurements using a six-component internal strain-gage balance[8] were performed in the same wind tunnel. The free-stream turbulence level is 0.08%. The variation of the the wind speed is within ± 0.5 m/s. The variation of the free-stream velocity direction is within $\pm 0.5^\circ$. The accuracy of α and β measurements is within $\pm 0.09^\circ$.

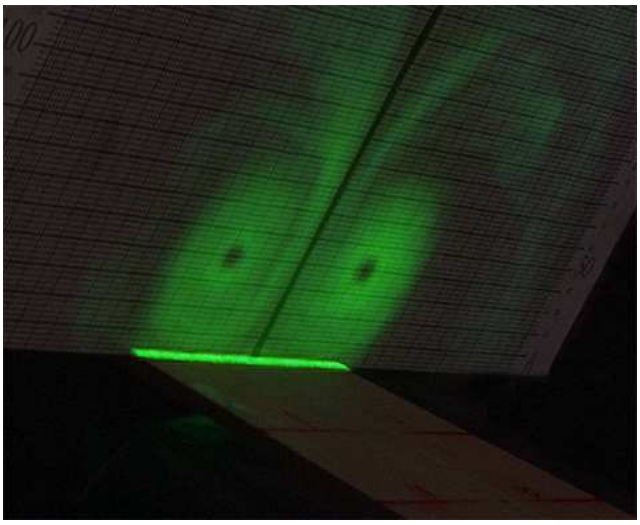

(a) wing alone

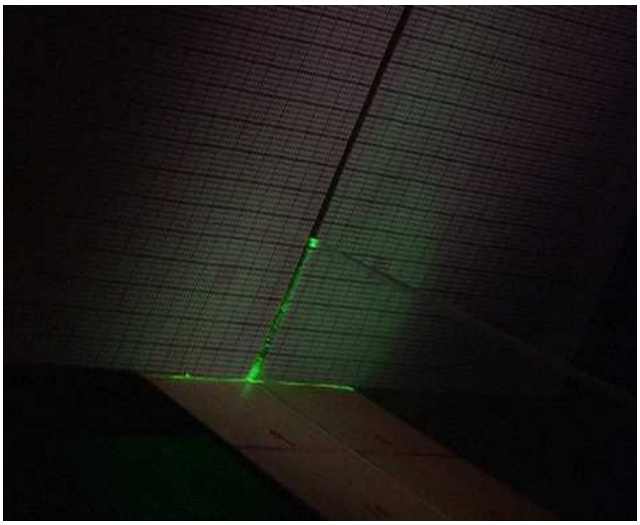

(b) wing+0.75s-fin

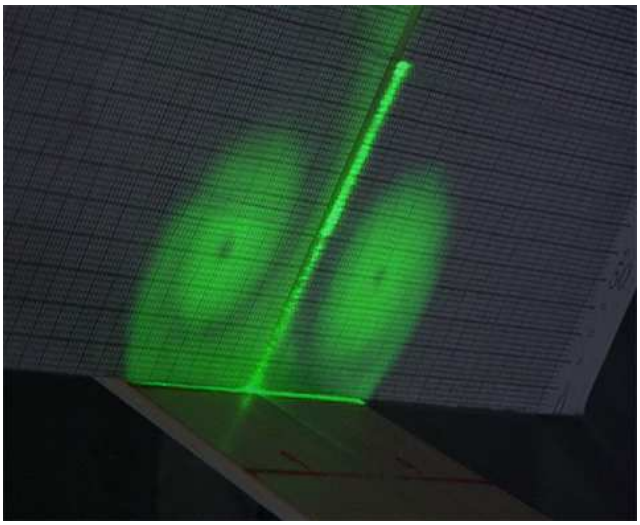

(c) wing+1.5s-fin

Figure 3. Photographs of cross flow overlapped with measuring grid at $\alpha = 29.02°$, $\beta = 0$, $x/c_0 = 0.54$ for the three models.

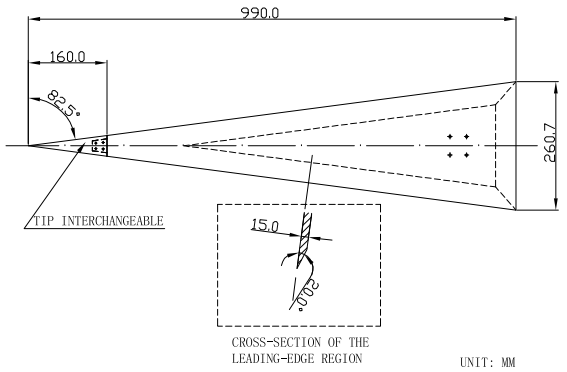

(a) wing alone

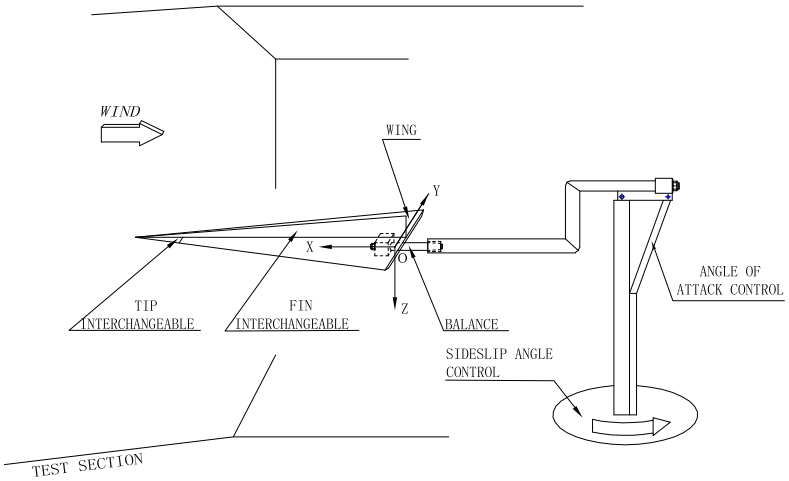

(b) test-section layout

Figure 4. Wing model and test-section layout for the force measurements.

The delta wing of 82.5° swept angle is made of aluminum alloy plate of thickness 15 mm as shown in Fig. 4. $c_0 = 990.0\ mm$. All edges are beveled with a 20° angle from the windward side of the wing so that the leeward side is perfectly flat. The two fins, $h_L/s = 0.3$ and 0.6 are made of aluminum alloy plate of thickness 2.0 mm. The fin leading edge is sharpened symmetrically with a 45° angle from both sides. The tip portion of the two models up to a station of 160.0 mm along the wing root chord is separately made to increase the precision in forming an accurate conical nose as assumed by the theory. The rest portion of the wing is common to the three models. The fin is fixed vertically on the upper surface of the wing in its symmetry plane. The test section layout is described in Fig. 4. The six aerodynamic components are referred to a balance coordinate system XYZ. The origin is set at the balance center which is located in the model symmetry plane. The X-axis points upstream, parallel to the wing root chord. The Y-axis points to the wing starboard side. The Z-axis points downward.

The tests are conducted at $\alpha = 12° \sim 32°$, $U_\infty = 35\ m/s$, $Re = 2.33 \times 10^6$. Figure 5 presents the yawing moment coefficient C_n versus α at zero sideslip for the wing-alone, the wing+0.3s-fin and the wing+0.6s-fin models from seven repeat runs.[8] The repeatability are fairly good. Similar results are obtained for the side force and rolling moment. A force asymmetry onsets at $\alpha = 26°$ and 22° for the wing+0.3s-fin and the wing+0.6s-fin model, respectively, and no asymmetry occurs for the wing model, which agrees with the theoretical predictions.[6]

V. Experimental Setup for PIV Study

The PIV experiments were conducted in a low-turbulence and low-noise 1.5 $m \times 1.5\ m$ wind tunnel at Beijing University of Aeronautics and Astronautics. The free-stream turbulence level is 0.08%. The wing and the wing+0.6s-fin models are those used in the force-measurement experiments.[8] The model support is enforced by suspending the model with tension wires to the wind tunnel wall. The wing body coordinates xyz are introduced for the PIV study. The origin is located at the wing apex, the x-axis points downstream and parallel to the wing root chord, the y-axis points to the wing starboard side and the z-axis points upward.

The PIV system is manufactured by DANTEC Company. Fig. 6 shows a schematic of the experimental setup. The Nd-YAG laser, a product of LABest Company PIV-350, emits double pulses of 350 mJ energy. Through optics, the laser beam is converted into a $220 \times 220\ mm$ light sheet of 3 mm thickness. The laser sheet is set normal to the wing root chord at various locations on the wing. The flow seeds are the smoke particles of approximately 1 μm in diameter commonly used in cinema industry. A CCD camera of 2048×2048 pixels is used to record the cross-flow fields. For each cross-flow field a dual-pulse separated with 30 μs is recorded 50 times at a frequency of 2 Hz. The dual-pulse images are analyzed with the FlowManager software to yield the distribution of the instantaneous velocity vector (v, w) over the cross-flow plane. The instantaneous vorticity component ω_x is calculated from the (v, w) distribution. The instantaneous values of (v, w) and ω_x are time-averaged over the 50 records in the time span 25 s.

VI. Experimental Results of PIV Study at $\alpha = 30°$

The PIV measurements are made at various cross-flow planes from $x/c_0 = 0.3$ to 0.8 with an increment of 0.1 for the wing+0.6s-fin model at $\alpha = 30°$, $K \approx 4.0$, $\beta = 0$, $U_\infty = 35\ m/s$, and $Re = 2.33 \times 10^6$.

For the wing-alone model the asymmetric flow is well known. For example, Stahl et al.[5] observed that the leading-edge vortices are symmetric, Verhaagen et al.[10] using a no-nulling five-hole probe showed that the cross-flow velocity components are conical away from the apex and trailing edge regions, and Visser, et al.[11] showed that the axial vorticity is also conical by cross-wire measurements. Thus, only one station at $x/c_0 = 0.6$ is measured for the wing model, while for the wing-fin model a series of stations are studied. No vortex breakdown on the wing surface is observed in the present experiments.

A. Comparison between the Wing and the Wing-Fin Models at $x/c_0 = 0.6$

Figure 7 shows the distribution of the time-averaged cross-flow velocity vector (v, w) for the wing model and the wing+0.6s-fin model at the station $x/c_0 = 0.6$. At the right top conner of the figure the free-stream velocity $U_\infty = 30\ m/s$ is ploted in scale. The maximum cross-flow velocity reaches nearly 75 m/s, which is higher than twice of the free-stream velocity.

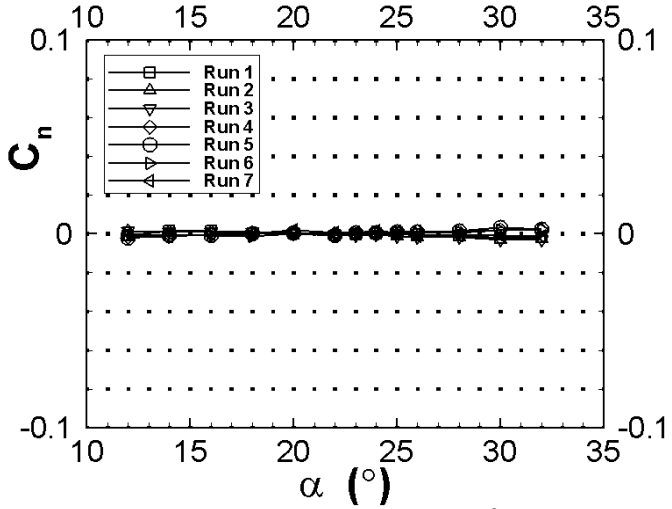

(a) wing alone, $Re = 1.66 \times 10^6$

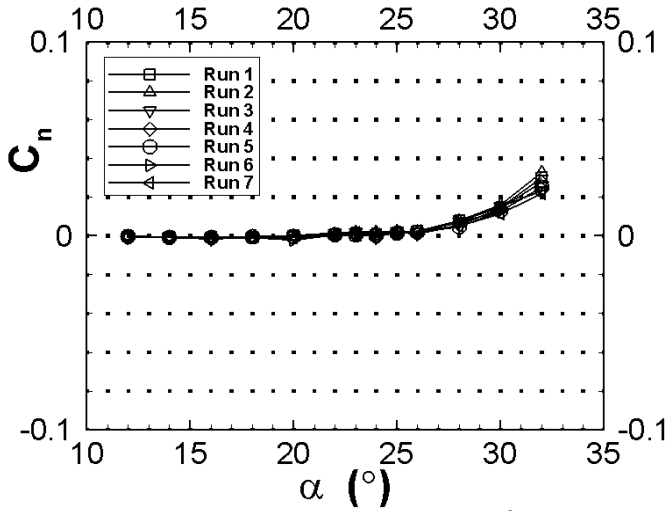

(b) wing+0.3s-fin, $Re = 2.33 \times 10^6$

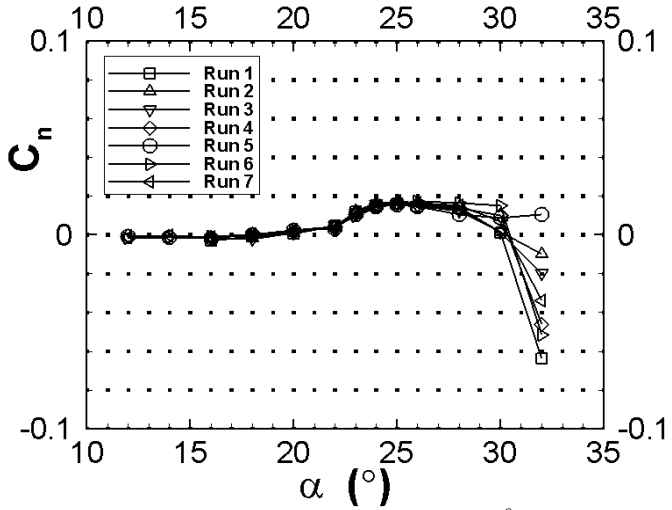

(c) wing+0.6s-fin, $Re = 2.33 \times 10^6$

Figure 5. Comparison of yawing-moment coefficients vs. α from seven repeat tests at $\beta = 0$.

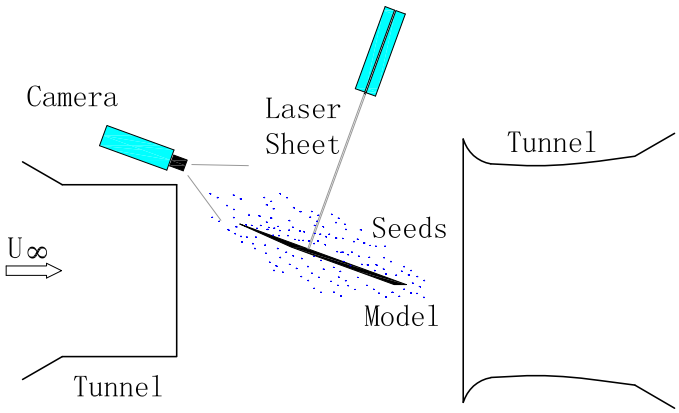

Figure 6. Schematic of the PIV experimental setup.

Figure 8 shows the contours of the time-averaged axial vorticity ω_x on the cross-flow plane for the wing model and the wing+0.6s-fin model at $x/c_0 = 0.6$. The free shear layer separated from the sharp leading edge of the wing first extends upward and outbound of the wing and then coils up spirally and finally develops into the concentric circular contours of a vortex core. The magnitude of the axial vorticity increases to maximum at the core center where the cross-flow velocity vanishes. (Compare with Figure 7.)

Table 2 presents the coordinate $(y/s, z/s)$ of the (primary) vortex center and the axial vorticity at the starboard and port vortex centers from Figure 8 for the wing and the wing-fin models. The magnitudes of the axial vorticity at the starboard and port vortex centers are substantially different for the wing-fin model, while those for the wing-alone model are practically the same. Therefore, the axial-vorticity distribution over the wing+0.6s-fin model is asymmetric to the symmetry plane of the model. The z/s-coordinates also indicates the asymmetry for the wing-fin model. The PIV study confirms the analytical predictions.[6]

Table 2. Comparison of the vortex center coordinates $(y/s, z/s)$ and the axial vorticity at the vortex center between the wing and the wing+0.6s-fin models at $x/c_0 = 0.6$, $\alpha = 30°$, $\beta = 0$.

Model	Port side			Starboard side		
	y/s	z/s	$\omega_x(1/sec)$	y/s	z/s	$\omega_x(1/sec)$
Wing	−0.69	0.59	−19475	0.69	0.63	19348
Wing+0.6s-fin	−0.73	0.54	−11804	0.73	0.64	14525

B. Chordwise Distributions of Axial Vorticity over the Wing-Fin Model

Chordwise development of the cross flow over the wing+0.6s-fin model are studied. Fig. 9 presents the contours of the time-averaged axial vorticity of the starboard vortex on the cross-flow planes from $0.3c_0$ to $0.8c_0$.

To study the flow conicity, the local semi-span s is chosen to normalize the axial vorticity. Table 3 presents the distribution of the non-dimensional axial vorticity $s\omega_x/U_\infty$ along the vortex center line and the coordinates $(y/s, z/s)$ of the vortex center over the wing+0.6s-fin model at Stations $x/c_0 = 0.3 - 0.8$. The positions of the two primary vortex center lines are definitely asymmetric, and the axial vorticity distributions along the two vortex center lines are significantly different. Thus, the symmetric vortex flow over the wing alone becomes asymmetric for the wing-fin model.

Table 3. Distribution of the axial vorticity $s\omega_x/U_\infty$ along the vortex center line and the center coordinates $y/s, z/s$ over the wing+0.6s-fin model at $x/c_0 = 0.3 - 0.8$, $\alpha = 30°$, $\beta = 0$.

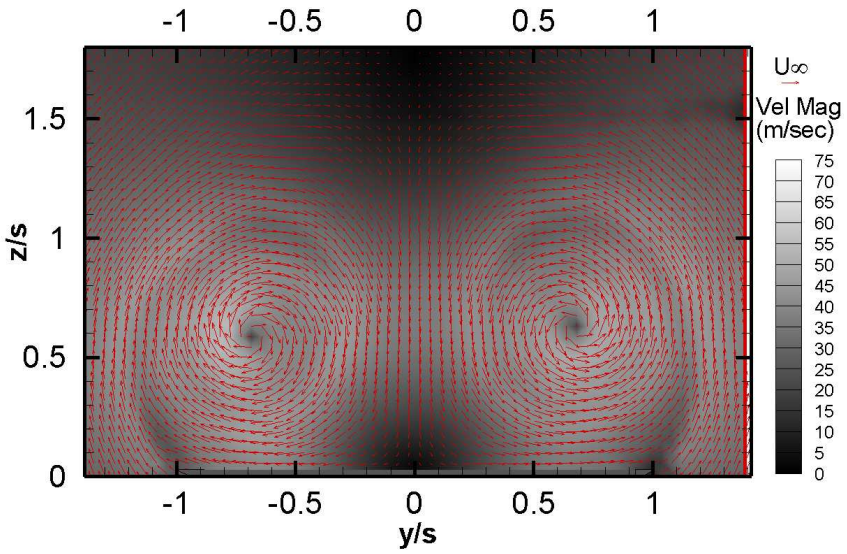

(a) wing-alone

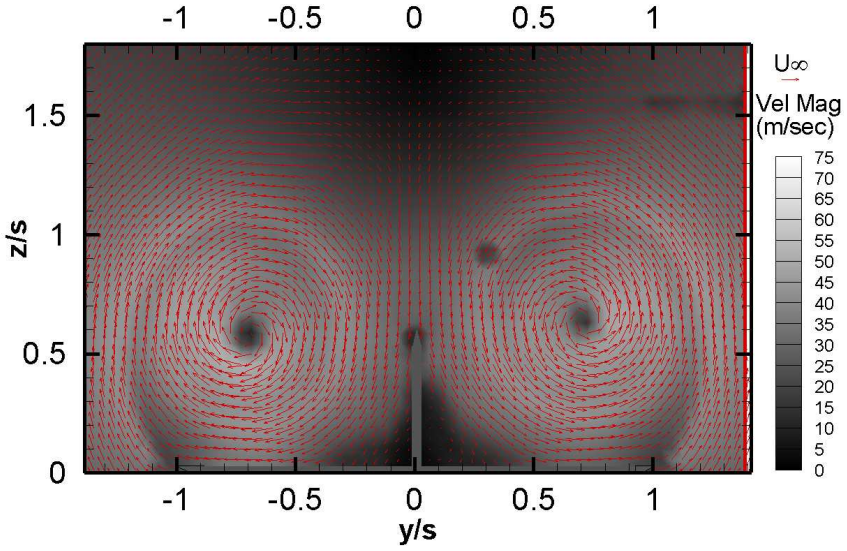

(b) wing+0.6s-fin

Figure 7. Comparison of the time-averaged velocity vector distributions between the wing and wing-fin models on the cross-flow plane at $x/c_0 = 0.6$, $\alpha = 30°$, $\beta = 0$.

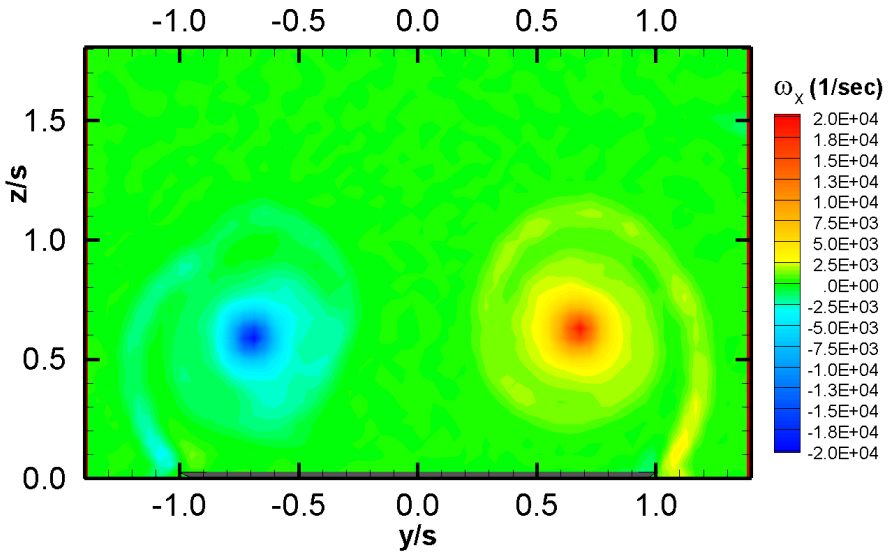

(a) wing-alone

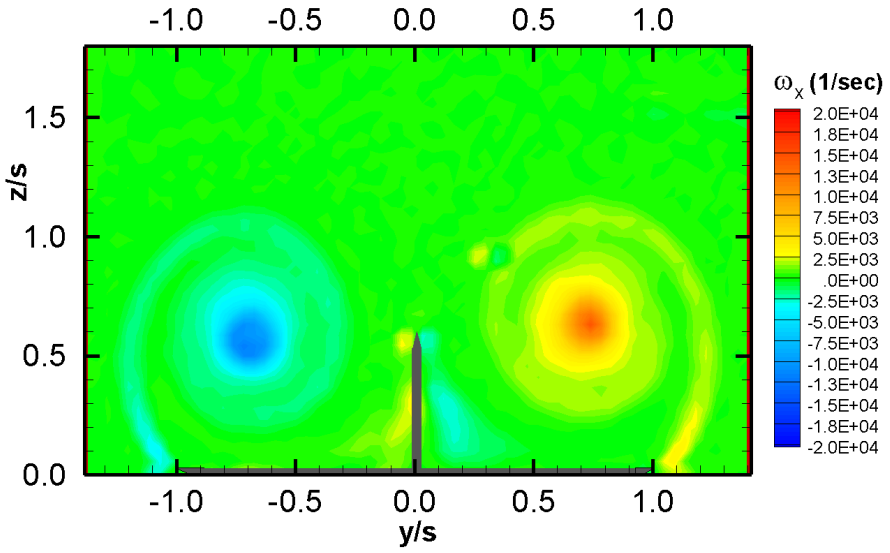

(b) wing+0.6s-fin

Figure 8. Comparison of the time-averaged axial vorticity contours between the wing and the wing-fin models on the cross-flow plane at $x/c_0 = 0.6$, $\alpha = 30°$, $\beta = 0$.

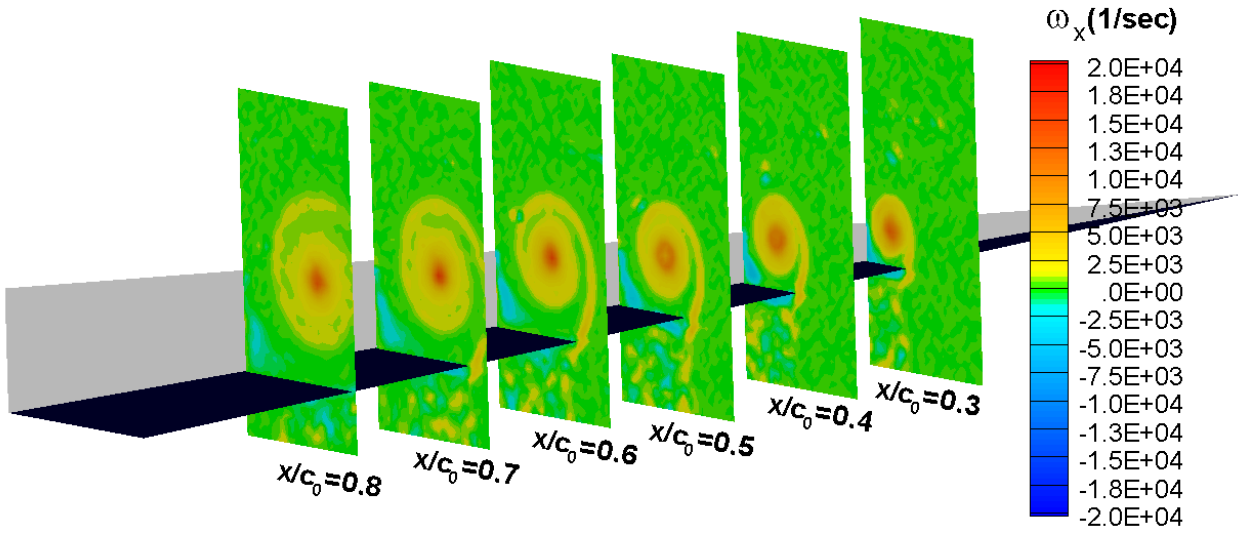

Figure 9. Contours of the time-averaged axial vorticity of the starboard vortex on the cross-sections $x/c_0 = 0.3 - 0.8$ for the wing+$0.6s$-fin model at $\alpha = 30^\circ$, $\beta = 0$.

	Port side			Starboard side		
x/c_0	$s\omega_x/U_\infty$	y/s	z/s	$s\omega_x/U_\infty$	y/s	z/s
0.3	−13.5	−0.72	0.46	14.2	0.72	0.54
0.4	−16.7	−0.79	0.51	15.7	0.81	0.58
0.5	−19.7	−0.77	0.46	18.1	0.72	0.46
0.6	−26.4	−0.73	0.54	32.5	0.73	0.64
0.7	−42.6	−0.70	0.59	39.4	0.70	0.59
0.8	−46.1	−0.72	0.58	38.3	0.71	0.60

To study the flow conicity two ray lines passing through the apex of the wing-fin model are chosen in the neighborhood of the vortices. Table 4 shows that the distribution of the non-dimensional axial vorticity along each ray line varies significantly with x/c_0 at $x/c_0 = 0.3 - 0.8$, $\alpha = 30°$, $\beta = 0$. Therefore, the conical flow over the wing alone becomes non-conical over the wing-fin model.

Table 4. Distribution of the axial vorticity $s\omega_x/U_\infty$ along two ray lines passing through the wing+0.6s-fin model apex at $x/c_0 = 0.3 - 0.8$, $\alpha = 30°$, $\beta = 0$.

	Port side			Starboard side		
x/c_0	$s\omega_x/U_\infty$	y/s	z/s	$s\omega_x/U_\infty$	y/s	z/s
0.3	−9.9	−0.73	0.54	8.8	0.73	0.64
0.4	−14.8	−0.73	0.54	13.4	0.73	0.64
0.5	−16.4	−0.73	0.54	15.2	0.73	0.64
0.6	−26.4	−0.73	0.54	32.5	0.73	0.64
0.7	−26.6	−0.73	0.54	27.0	0.73	0.64
0.8	−35.2	−0.73	0.54	32.4	0.73	0.64

The existence of asymmetric flow for the slender wing-fin model at high angles of attack and zero sideslip provides a new aerodynamic forebody configuration for lateral-force control of high-performance air vehicles, like the slender pointed forebody of revolution.[12] Future plans include exploration of the inherent bi-stable vortex nature of the wing and low dorsal fin combination and the possible dynamic manipulation of the vortices over the wing-fin model.

VII. Conclusions

The stability of vortices over a slender sharp leading-edged flat-plate delta wing with and without a dorsal fin mounted in the symmetry plane of the wing at high angles of attack, zero sideslip and low speed is analyzed and tested. The analysis is based on a linearized stability theory and a slender conical-flow model. The experimental studies by smoke-laser-sheet visualization, six-component strain gage measurement and particle image velocimetry are performed in parallel with the analytical results.

The distributions of the time-averaged axial vorticity component obtained from a particle image velocimetry study clearly demonstrate that the vortical flow over the wing with the low dorsal fin at a high angle of attack is asymmetric and non-conical. Therefore, the stable symmetric vortex pair over a slender sharp-edged flat-plate delta wing becomes unstable under small perturbations when combined with a flat-plate dorsal fin of low height. Exploration of the inherent bi-stable vortex nature of the wing-fin model is suggested.

Acknowledgments

The present work is supported by the Foundation for Fundamental Research of the Northwestern Polytechnical University, NPU-FFR-W018101. The authors are grateful to Professor Xueying Deng of Beijing University of Aeronautics and Astronautics for their assistance in using the PIV system and the wind tunnel.

References

[1]Ericsson, L., "Sources of high alpha vortex asymmetry at zero sideslip," *Journal of Aircraft*, Vol. 29, No. 6, Nov-Dec 1992, pp. 1086–1090.

[2]Shanks, R., "Low-subsonic measurements of static and dynamic stability derivatives of six flat-plate wing having leading-edge sweep angles of 70° to 84°," NASA TN D-1822, July 1963.

[3]Polhamus, E., "Predictions of vortex-lift characteristics by a leading-edge suction analogy," *Journal of Aircraft*, Vol. 8, 1971, pp. 193–199.

[4]Keener, E. and Chapman, G., "Similarity in vortex asymmetries over slender bodies and wings," *AIAA Journal*, Vol. 15, No. 9, 1977, pp. 1370–1372.

[5]Stahl, W., Mahmood, M., and Asghar, A., "Experimental investigations of the vortex flow on delta wings at high incidence," *AIAA Journal*, Vol. 30, 1992, pp. 1027–1032.

[6]Cai, J., Liu, F., and Luo, S., "Stability of symmetric vortices in two-dimensions and over three-dimensional slender conical bodies," *J. Fluid Mech.*, Vol. 480, No. 4, April 2003, pp. 65–94.

[7]Meng, X., Qiao, Z., Gao, C., Luo, S., and Liu, F., "Visualization of vortex flow over delta wing with dorsal fin," AIAA Paper 2005-1058, Jan. 2005.

[8]Meng, X., Jia, C., Qiao, Z., Gao, C., Luo, S., and Liu, F., "Aerodynamic characteristics of slender delta wing with low dosal fin," AIAA Paper 2007-1272, Jan. 2007.

[9]Sychev, V., "Three-dimensional hypersonic gas flow past slender bodies at high angle of attack," *Journal of Math. and Mech. (USSR)*, Vol. 24, Feb. 1960, pp. 296–306.

[10]Verhaagen, N. and Kruisbrink, A., "Entrainment effect of a leading-edge vortex," *AIAA Journal*, Vol. 25, No. 8, Aug., 1987, pp. 1025–1032.

[11]Visser, K.D. and Nelson, R.C., "Measurements of circulation and vorticity in the leading-edge vortex of a delta wing," *AIAA Journal*, Vol. 31, No. 1, Jan., 1993, pp. 104–110.

[12]Malcolm, G., "Forebody vortex control," *Prog. Aerospace Sci.*, Vol. 28, 1991, pp. 171–234.